

Table S1. The chemical compositions of Zn-N-MoC-H obtained by XPS and EDS.

Content Element	C	Mo	N	Zn	O
XPS (at.%)	66.61	5.86	12.43	0.4	14.7
XPS (wt.%)	44.48	31.29	9.68	1.46	13.09
EDS (wt.%)	57.17	32.97	0.45	2.41	6.99

Table S2. Summary of representative Mo-based HER catalysts in 0.5 M H₂SO₄ electrolyte.

Catalyst	η_0^a	Ts ^b	η_{10}^c	References
Zn-N-MoC-H NSs	-66	52.1	128	This work
Mo ₂ C/hierarchical carbon microflowers	-85	55	144	<i>ACS Nano</i> 2016 , <i>10</i> , 11337.
N-doped C@MoS ₂ nanoboxes	~-100	55	165	<i>Angew. Chem. Int. Ed.</i> 2015 , <i>54</i> , 7395.
MoC _x nano-octahedrons	-87	53	142	<i>Nat. Commun.</i> 2015 , <i>6</i> , 6512.
Mo ₂ C/graphitic carbon sheets	-120	62.6	200	<i>ACS Catal.</i> 2014 , <i>4</i> , 2658.
β -Mo ₂ C nanotubes	-82	62	172	<i>Angew. Chem. Int. Ed.</i> 2015 , <i>54</i> , 15395.
Mo ₂ C nanowires	-70	53	200 ^d	<i>Energy Environ. Sci.</i> 2014 , <i>7</i> , 387.
Mo ₂ C-WC composite nanowires	~-80	52	~135	<i>Adv. Funct. Mater.</i> 2015 , <i>25</i> , 1520.
N, P-Mo ₂ C@C	~-100	56	141	<i>ACS Nano</i> 2016 , <i>10</i> , 8851.
Mo ₂ C/3D N-doped carbon nanofiber	-105	70	192	<i>NPG Asia Mater.</i> 2016 , <i>8</i> , e288.
Mo ₂ C-carbon sphere	-100	85	164	<i>Nano Energy</i> 2017 , <i>32</i> , 511.

^a Onset potential obtained at -1 mA cm⁻² (mV vs. RHE);

^b Tafel slope (mV dec⁻¹);

^c Overpotential obtained at -10 mA cm⁻² (mV vs RHE).

^d η_{60}

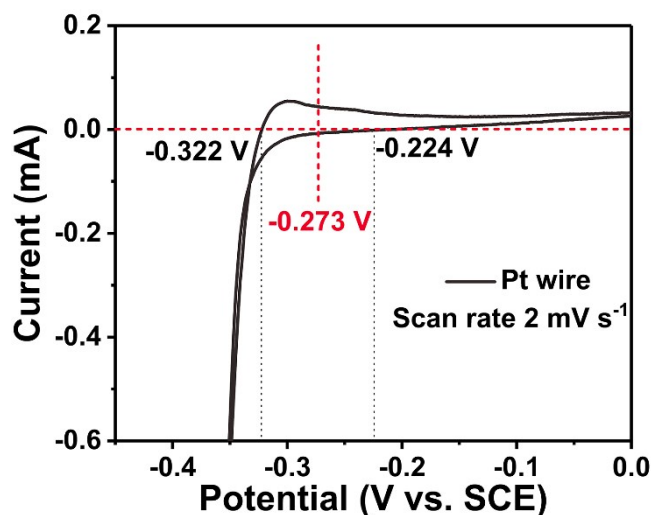


Figure S1. RHE voltage calibration CV curve.

The calibration was performed in a high-purity H_2 (99.999 %) saturated electrolyte with a Pt wire as the working electrode and counter electrode. Cyclic voltammograms (CVs) were collected at a scan rate of 2 mV s^{-1} , and the average of the two potentials at which the current crossed zero was taken as the thermodynamic potential for the hydrogen electrode reactions. In $0.5 \text{ M H}_2\text{SO}_4$, $E(\text{SCE}) = E(\text{RHE}) + 0.273 \text{ V}$.

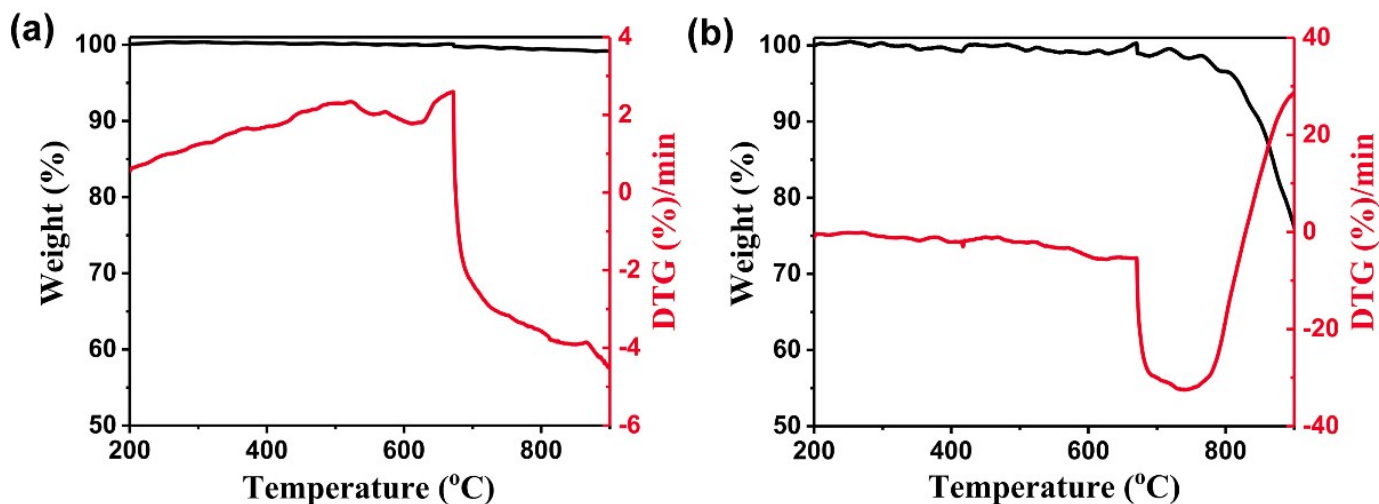


Figure S2. DTA-TG pattern of (a) $\text{ZnO}/\text{Zn}_2\text{Mo}_3\text{O}_8$ and (b) Zn .

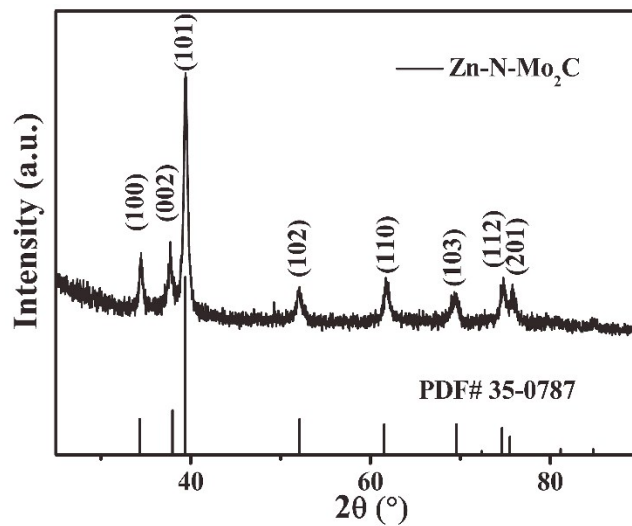


Figure S3. XRD pattern of Zn-N-Mo₂C.

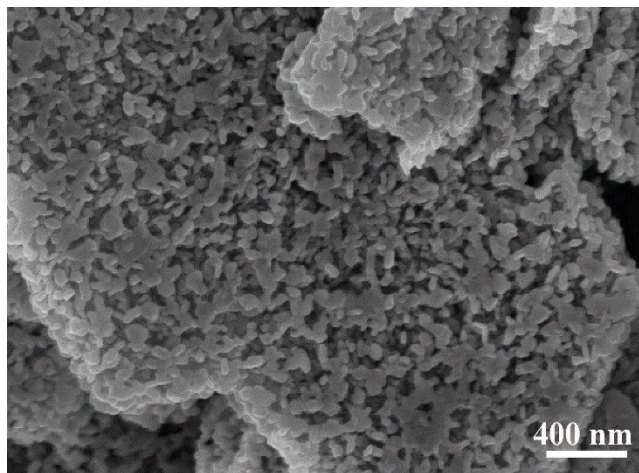


Figure S4. SEM image of ZnMoO₄ calcined under Ar/H₂ (10 vol% H₂) at 650 °C for 2 h.

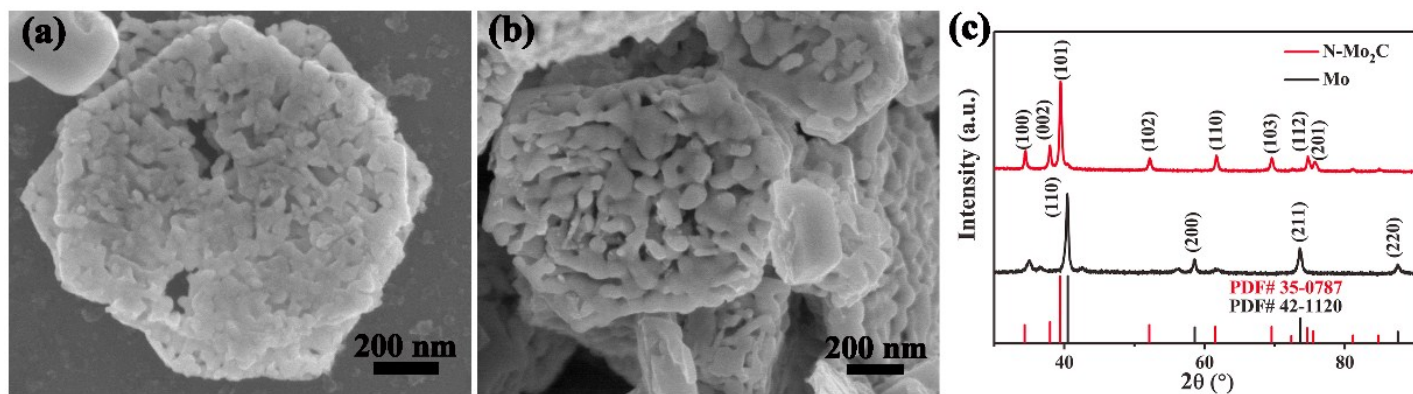


Figure S5. SEM image of (a) pure Mo nanosheets, (b) N-MoC nanosheets and (c) XRD patterns.

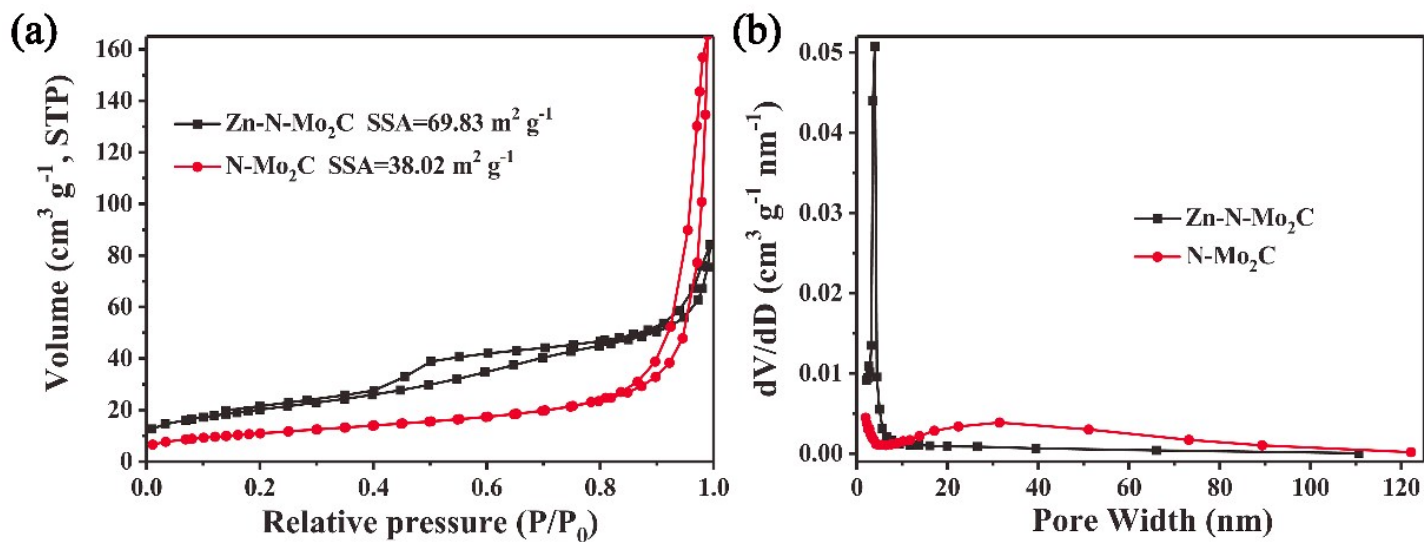


Figure S6. (a) The nitrogen adsorption-desorption isotherms and (b) pore size distributions of Zn-N-Mo₂C and N-Mo₂C.

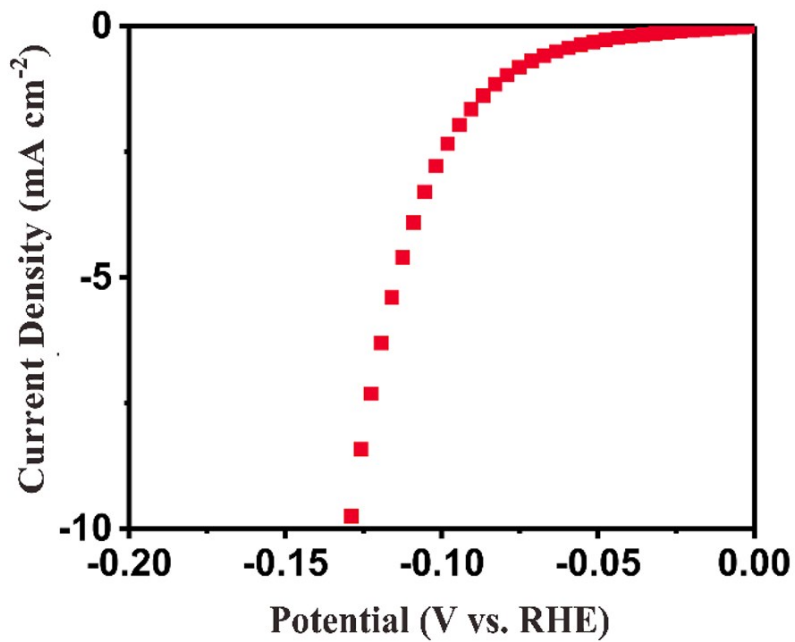


Figure S7. Partial enlarged view of polarization curves (with iR correction) of Zn-N-MoC-H.

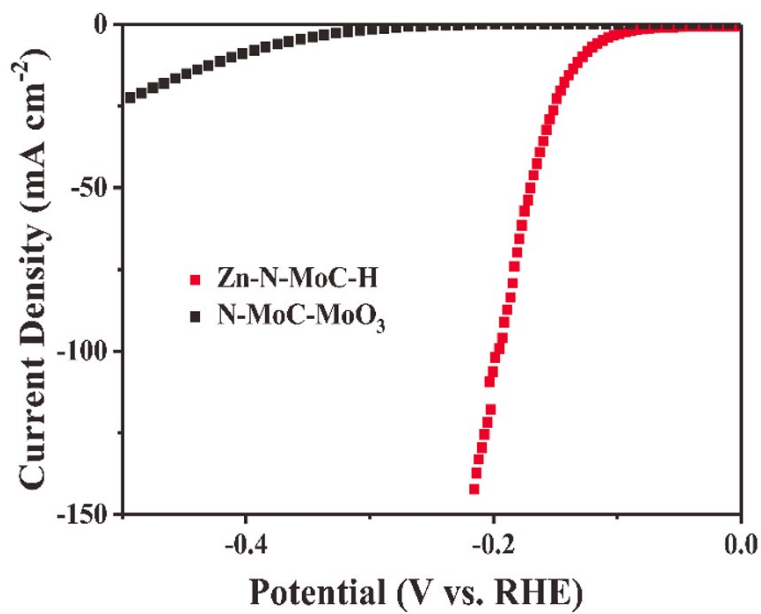


Figure S8. Polarization curves (with iR correction) of Zn-N-MoC-H and N-MoC-MoO₃.

Reduction temperature and time:

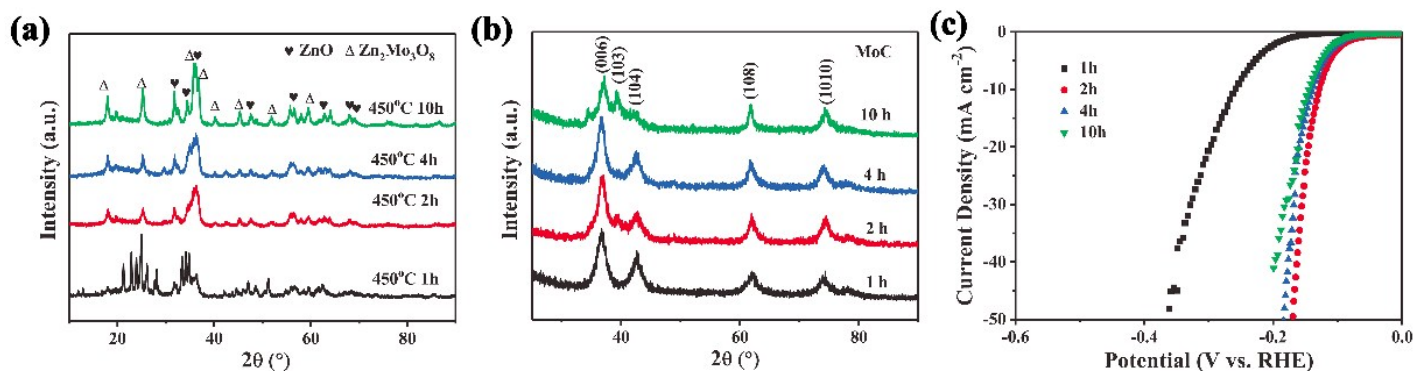


Figure S9. XRD patterns of H₂ reduced ZnMoO₄ at 450 °C for different times (a), the corresponding carbides synthesized at the same condition of 800 °C, 2h (b) and polarization curves (c).

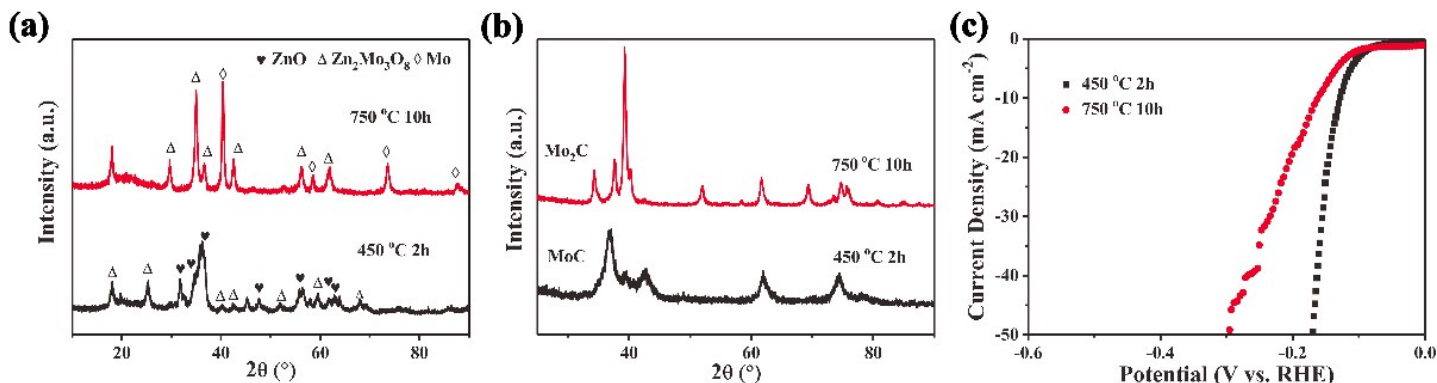


Figure S10. XRD patterns of H₂ reduced ZnMoO₄ at 450 °C for 2 h and 750 °C for 10 h (a), the corresponding carbides synthesized at the same condition of 800 °C, 2h (b) and polarization curves (c).

The reduction temperature obviously affected the phase transformation of obtained molybdenum carbide and produced the different HER activities. At the 450 °C for more 2h, the ZnO/Zn₂Mo₃O₈ can be synthesized and then form the MoC after calcination with dicyandiamide. Therefore, the existence of ZnO in ZnMoO₄ promoted the synthesis of MoC instead of Mo₂C, which results in enhanced HER performance. In order to remove ZnO, at the higher reduced temperature at 750 °C for 10 h, the Mo/Zn₂Mo₃O₈ was synthesized and then calcinated with dicyandiamide, which only produced Mo₂C with weaker HER activity. Therefore, the ZnO can modulate the crystalline phase (MoC) and crystal face (103) of molybdenum carbide, which caused the enhanced HER activity.

Calcination Temperature

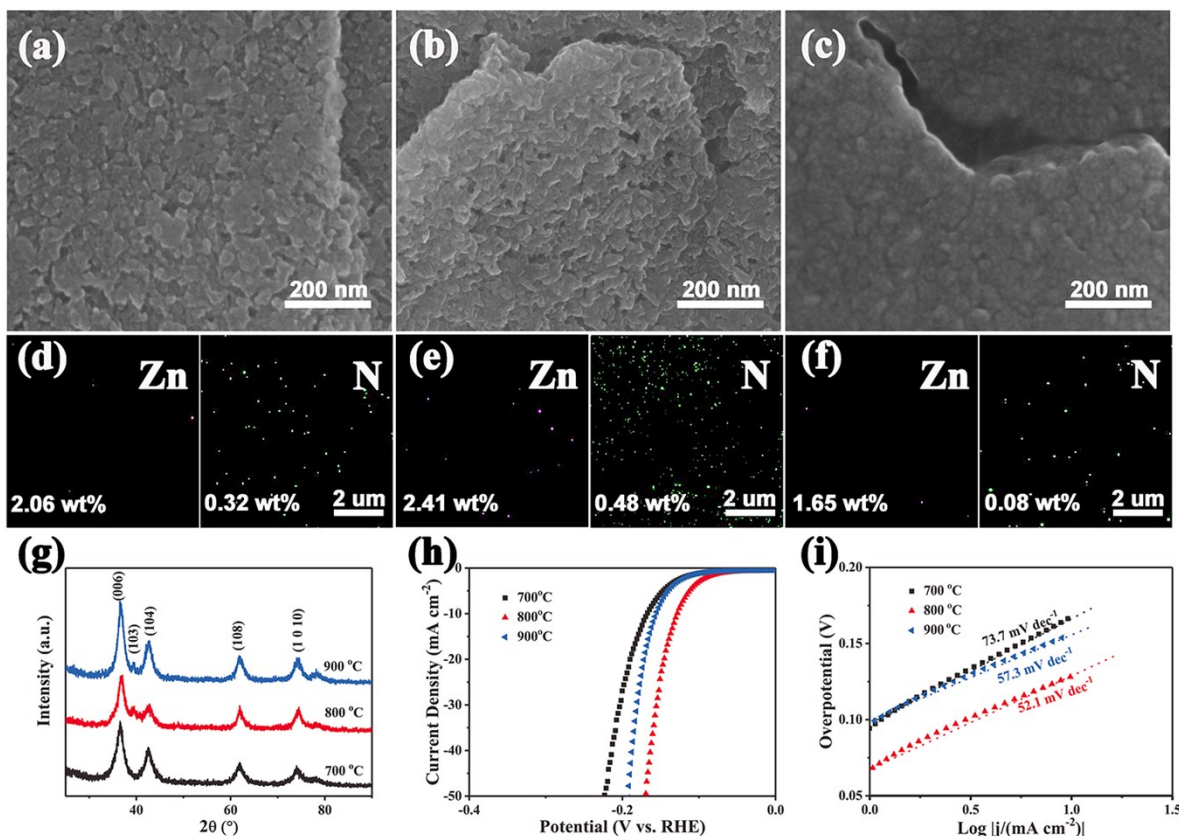


Figure S11. SEM images (a-c), EDS mapping (d-f), XRD (g), polarization curves (h) and (i) Tafel slopes of the samples synthesized with different temperatures (700 °C, 800 °C and 900 °C).

The different calcination temperatures (700 °C, 800 °C and 900 °C) were studied to determine the influence for Zn-N-MoC-H NSs. At all calcination temperatures, MoC was synthesized and the porous nanosheet morphology was retained. As shown in **Figure S10**, the sample obtained at 800 °C possessed the best HER activity with the onset potential of -66 mV and Tafel slope of 52.1 mV dec⁻¹, which was better than that of Zn-N-MoC-H NSs-700 °C (-97 mV, 73.7 mV dec⁻¹). Compared to the XRD, a new diffraction peak at 42.569° was detected at 800 °C, which is a possible active surface for HER. In addition, the Zn-N-MoC-H NSs obtained at 900 °C (-97 mV, 61.9 mV dec⁻¹) possessed the lowest HER activity due to the decreased Zn and N doping. The amount of Zn and N doping of samples obtained at different temperatures were characterized by EDS mapping in **Figure S10d-f**. Compared to Zn (2.41 wt%) and N (0.48 wt%) doping amounts in Zn-N-MoC-H NSs-800, the decreased doping amounts of Zn (1.65 wt%) and N (0.08 wt%) (Zn-N-MoC-H NSs-900) were attributed to the sublimation of Zn and decomposition of unstable doped N at high calcination temperature.

Dicyandiamide amount

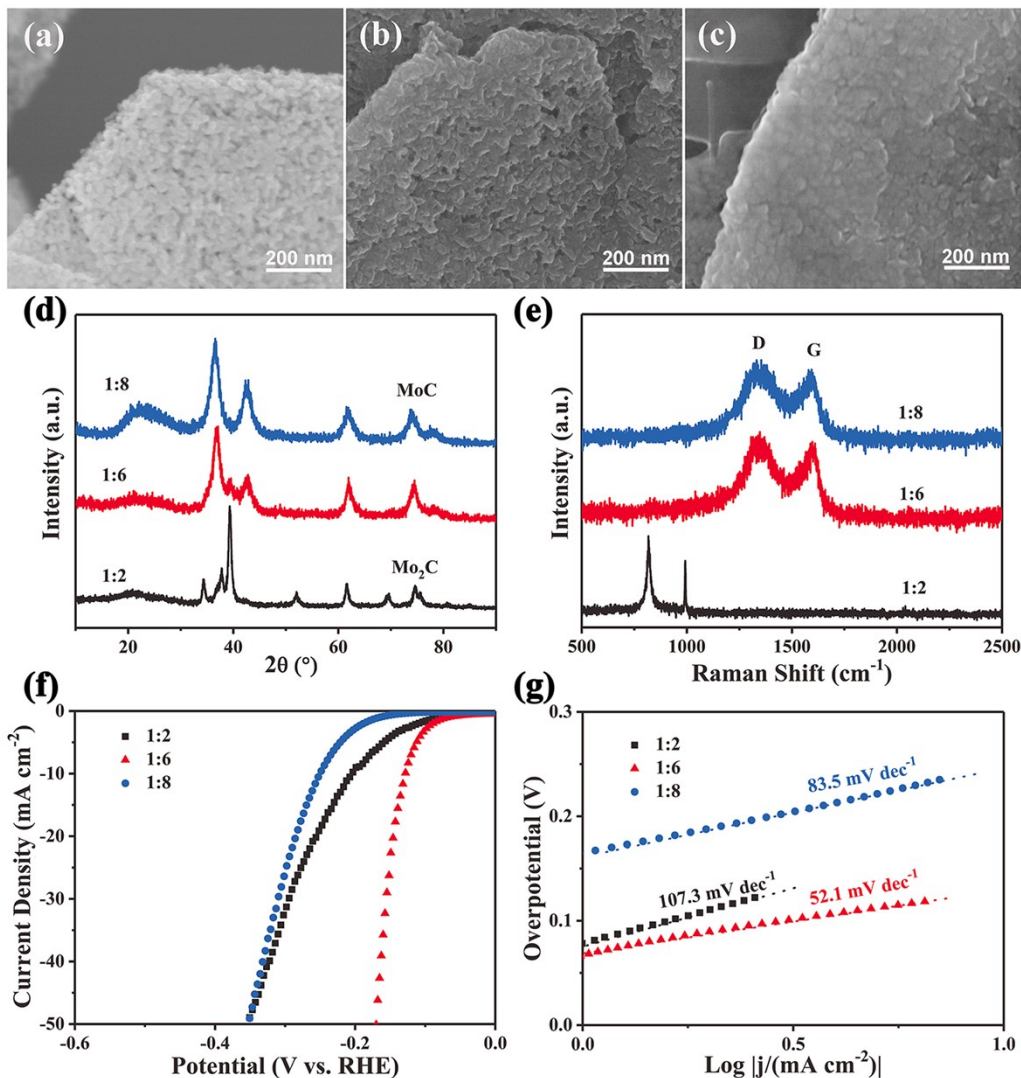


Figure S12. SEM images (a-c), XRD (d), polarization curves (e) and (f) Tafel slopes of the samples synthesized with different ratio of ZnO/Zn₂Mo₃O₈ and dicyandiamide (1:2, 1:6 and 1:8).

The amount of dicyandiamide and calcination temperature obviously affected the morphology, phase transformation and composition of obtained molybdenum carbide and produced different HER activities. The amount of dicyandiamide affected the crystalline phase and surface structure of molybdenum carbide during calcining process. The incomplete transformation from ZnO/Zn₂Mo₃O₈ NSs to Zn-N-Mo₂C-H NSs (PDF# 35-0787) was detected with lower dicyandiamide (1:2). Greater dicyandiamide (1:6) produced the MoC (PDF# 08-0384). The excess dicyandiamide (1:8), the amorphous carbon at 20 ~ 25° was detected by XRD. The polarization curves for HER showed the Zn-N-MoC-H NSs synthesized with the appropriate amount of dicyandiamide possessed the best HER performance, which needed not only successfully transformed ZnO/Zn₂Mo₃O₈ to Zn-N-MoC-H NSs, but also prevented excess carbon on the surface of MoC NSs produced from the more dicyandiamide covering the active sites of MoC

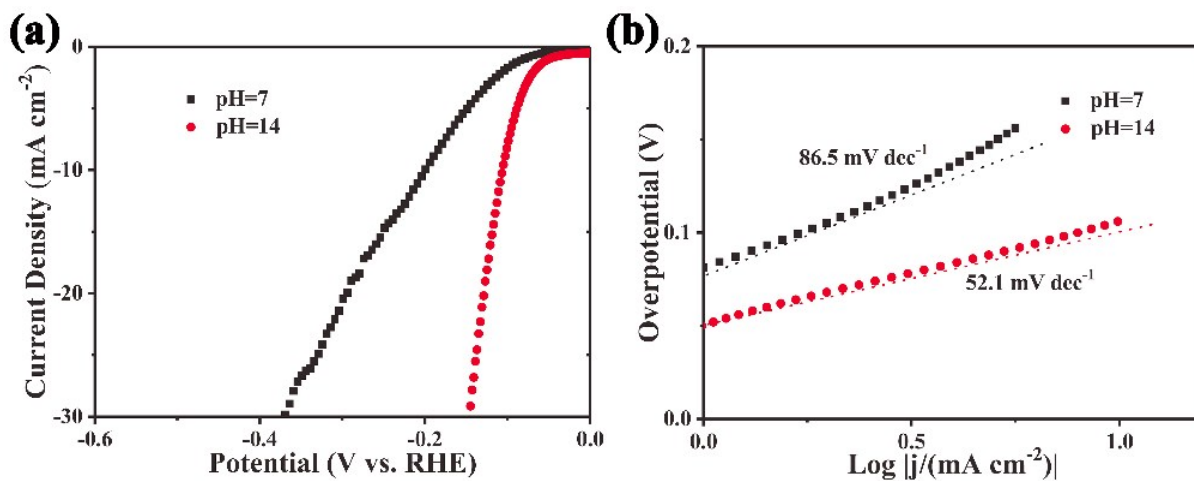


Figure S13. (a) Polarization curves (with iR correction) and (b) Tafel plots of Zn-N-MoC-H in 1.0 M KOH (pH=14), and 1.0 M phosphate buffered saline (pH=7).

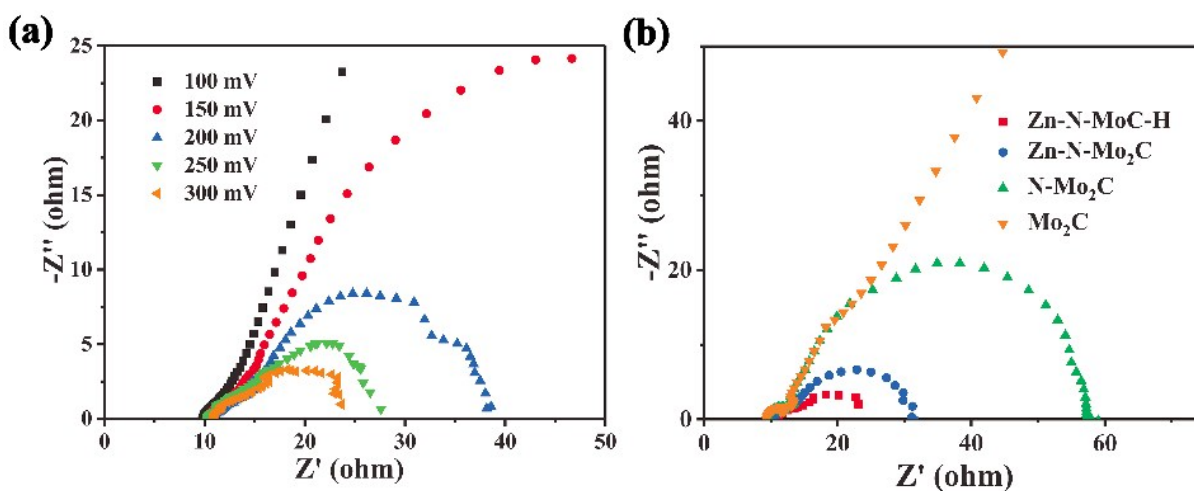


Figure S14. (a) Electrochemical impedance spectra of N-MoC at various HER overpotentials in 0.5 M H₂SO₄. (b) Electrochemical impedance spectra of Zn-N-MoC-H, Zn-N-Mo₂C, N-Mo₂C and Mo₂C at the same HER overpotential of 300 mV in 0.5 M H₂SO₄.

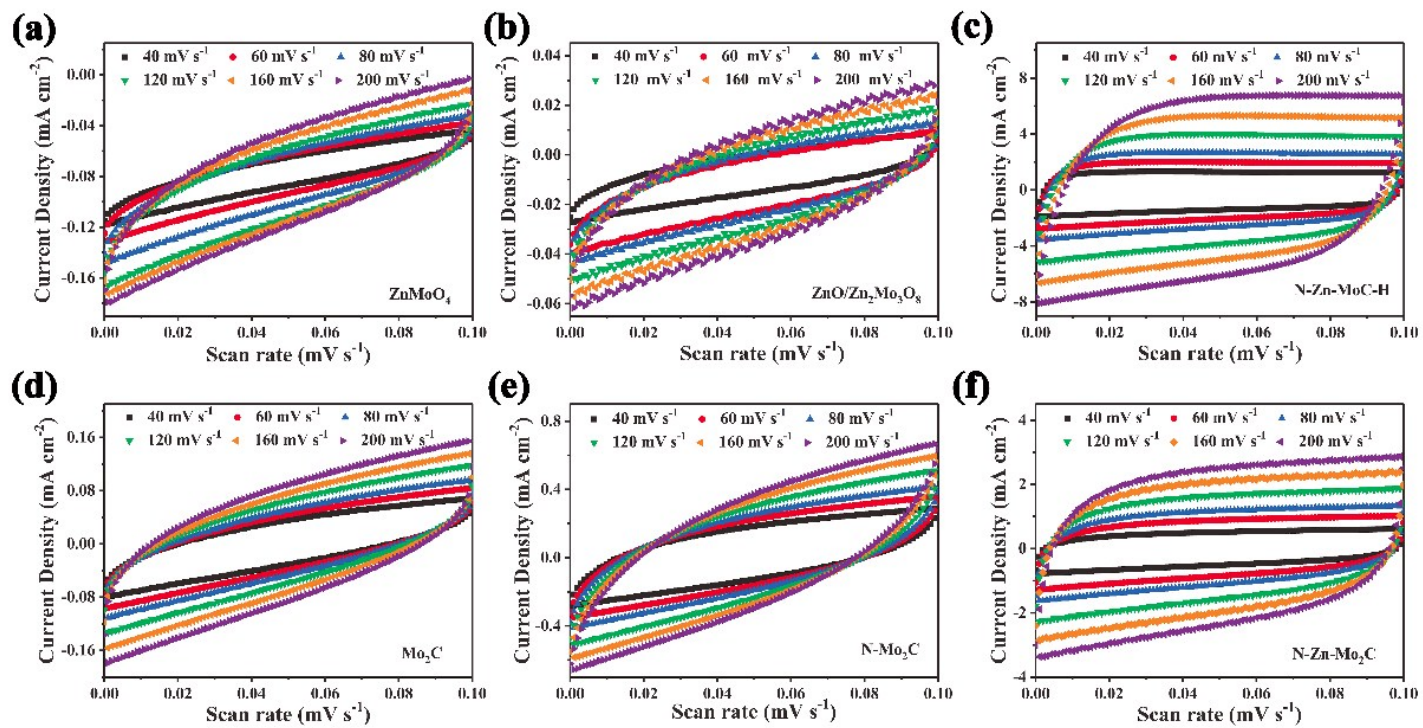


Figure S15. The cyclic voltammograms (CVs) curves of (a) ZnMoO_4 , (b) $\text{ZnO}/\text{Zn}_2\text{Mo}_3\text{O}_8$, (c) $\text{Zn-N-Mo}_2\text{C-H}$, (d) $\text{Zn-N-Mo}_2\text{C}$, (e) $\text{N-Mo}_2\text{C}$ and (f) N-MoC-MoO_3 .

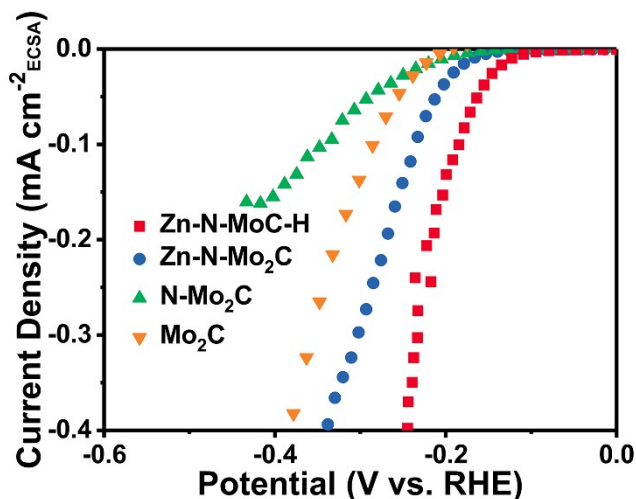


Figure S16. Amended polarization curves of Zn-N-MoC-H, Zn-N-Mo₂C, N-Mo₂C and Mo₂C obtained by normalizing the HER currents to the respective electrochemical active surface area.

The specific capacitance can be converted into an electrochemical active surface area (ECSA) using the specific capacitance value for a flat standard with 1 cm² of real area (**Figure 4d**). The specific capacitance for a flat surface is generally found to be in the range of 20-60 μF cm⁻². The ECSA was calculated according to the formula¹:

$$ECSA = \frac{Capacitance}{40 \mu F cm^{-2} per cm^{-2}_{ECSA}}$$

The ECSA of Zn-N-MoC-H, Zn-N-Mo₂C, N-Mo₂C and Mo₂C are 787.5 cm², 297.5 cm², 265 cm² and 17.5 cm², respectively. The polarization curves of these samples were amended according to ECSA to compare the HER performance of per unit ECSA. (**Figure S16**) For per unit ECSA, the Zn-N-MoC-H also exhibited the highest HER activity due to the Zn, N co-doping and the lower HER potential of Zn-N-Mo₂C than N-Mo₂C and Mo₂C also proved the effect of Zn-doping and N doping.

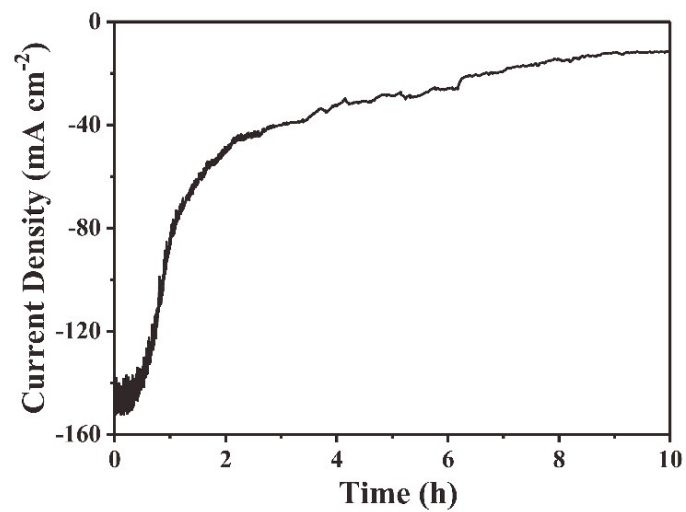


Figure S17. The i-t testing of 20 wt% Pt/C with an overpotential of 230 mV.

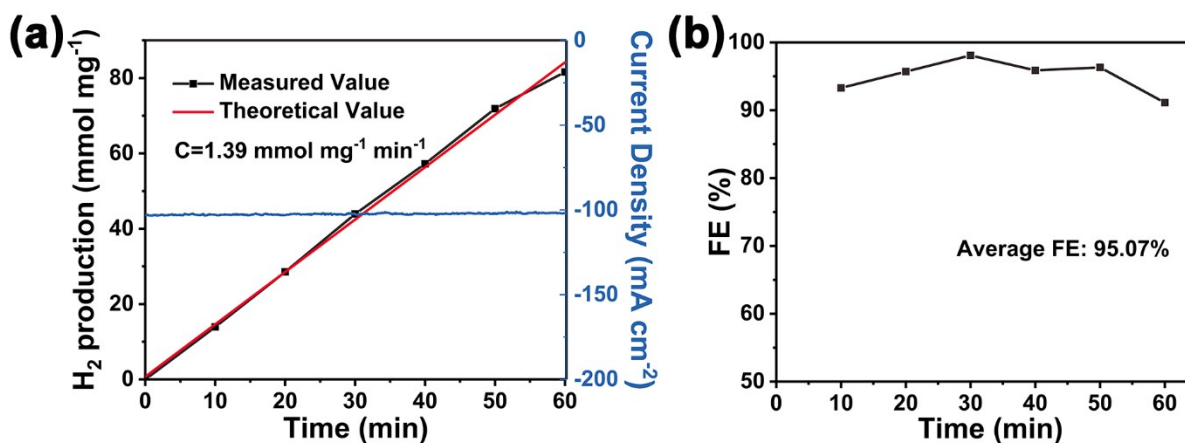


Figure S18. (a) Hydrogen production and (b) faradaic efficiency (FE) of the electrolyzer of the Zn-N-MoC-H obtained by gas chromatography with an overpotential of 200 mV at different reaction times.

Characterizations of gas chromatographic measurements and Faradaic efficiency (FE) calculations: Gas chromatographic measurements was performed on the GC-2060F (LuNan Analytical Instruments, LTD, China) to quantify the amount of hydrogen gas production. A custom-made sealed three electrode electrolytic cell was used and purged with N₂ gas for 30 min. The reaction was carried at a constant applied voltage (-200 mV vs RHE) for 1 h. The H₂ gas was collected by using a microsyringe of 1 mL from the cell in equal interval of time and injected into GC. The H₂ production was calculated according to the formula:

$$n_{H_2} = \frac{S_t}{S_s} \times \frac{V}{22.4}$$

where S_t was the peak area of H₂ tested by GC for 1 mL gas collected from the sealed cell, S_s was the peak area tested by 1 mL pure hydrogen (99.9%), V was the volume of the electrolytic tank minus that of the electrolyte.

For the Faradaic efficiency (FE), GC data for H₂ collected during the spanned of 10 min at constant voltage of (-200 mV vs RHE) in equal intervals were used to calculate the FE of HER according to following relationship:

$$FE = \frac{2F \times n_{H_2}}{Q}$$

where n_{H₂} is the amount of hydrogen generated, Q is the total amount of charge passed through the cell, and F is the faraday constant.

Reference:

[1] J. Kibsgaard, T. F. Jaramillo, *Angew. Chem., Int. Ed.*, 2014, 53, 14433–14437